Journal of Solid State Chemistry 192 (2012) 385–389

Contents lists available at SciVerse ScienceDirect

Journal of Solid State Chemistry

journal homepage: www.elsevier.com/locate/jssc

Structural phase transitions in the $Ag_2Nb_4O_{11}$–$Na_2Nb_4O_{11}$ solid solution

David I. Woodward *, Martin R. Lees, Pam A. Thomas

Department of Physics, University of Warwick, Gibbet Hill Road, Coventry CV4 7AL, UK

ARTICLE INFO

Article history:
Received 13 February 2012
Received in revised form
9 April 2012
Accepted 10 April 2012
Available online 17 April 2012

Keywords:
Ferroelectrics
Phase transitions
Natrotantites

ABSTRACT

The phase transitions between various structural modifications of the natrotantite-structured system $xAg_2Nb_4O_{11}$–$(1-x)Na_2Nb_4O_{11}$ have been investigated and a phase diagram constructed as a function of temperature and composition. This shows three separate phase transition types: (1) paraelectric–ferroelectric, (2) rhombohedral–monoclinic and (3) a phase transition within the ferroelectric rhombohedral zone between space groups $R3c$ and $R3$. The parent structure for the entire series has space group $R\bar{3}c$. Compositions with $x>0.75$ are rhombohedral at all temperatures whereas compositions with $x<0.75$ are all monoclinic at room temperature and below. At $x=0.75$, rhombohedral and monoclinic phases coexist with the phase boundary below room temperature being virtually temperature-independent. The ferroelectric phase boundary extends into the monoclinic phase field. No evidence was found for the $R3$–$R3c$ phase boundary extending into the monoclinic phase field and it is concluded that a triple point is formed.

1. Introduction

Ferroelectricity occurs in many different oxide groups. Of these, perovskites are by far the most widely studied, due in part to their simple prototype structure, the wide range of compounds that can be formed and their existing markets for applications. Ferroelectricity also exists in other oxide groups, such as tungsten bronzes [1], pyrochlores [2,3] and bismuth layered structures including Aurivillius phases [4]. These structures are all based on corner-sharing octahedra that are able to undergo distortions that can lead to the development of a switchable polarisation. However, some recent work has revealed that ferroelectricity exists in the material $Ag_2Nb_4O_{11}$ [5,6], one of a number of materials with structures related to the minerals natrotantite ($Na_2Ta_4O_{11}$) [7,8] and calciotantite ($CaTa_4O_{11}$) [9]. These materials are not based solely on corner-sharing octahedra, but are comprised of alternating layers of distorted edge-sharing TaO_7 or NbO_7 polyhedra which are corner-connected to layers containing regular TaO_6 or NbO_6 octahedra. The larger, lower valancy cations are incorporated into the layers with the regular octahedra and, in addition to Ag^+, Na^+ and Ca^{2+}, the cations Cu^+ [10,11], Sr^{2+} [12], and La^{3+} [13] are compatible with this structure, although the presence of La^{3+} requires charge-balancing by replacing some Ta^{5+} with Zr^{4+}. The majority of known phases with the natrotantite structure are formed with Ta^{5+}.

At present, only $Ag_2Nb_4O_{11}$ from this group of materials is known to be ferroelectric. It is rhombohedral at room temperature with space group $R3c$. Its Curie temperature, T_C, is $\sim$150 °C, where it goes through a phase transition to a paraelectric structure with space group $R\bar{3}c$. At $\sim$ −75 °C, there is another phase transition to a structure with space group $R3$ [5]. Evidence for the low-temperature phase transition was first seen in permittivity measurements [14] which displayed a shoulder at $\sim$ −100 °C. Structural refinements against neutron diffraction data showed an abrupt increase in volume between −75 and −50 °C and the space group $R3$ proved to be best for structural refinements at −100 °C and below [5]. At room temperature, $Na_2Nb_4O_{11}$ is monoclinic with the centrosymmetric space group $C2/c$, transforming to $R\bar{3}c$ at $\sim$80–100 °C [15,16]. No phase transitions at lower temperatures are known and therefore no ferroelectric phase exists for this compound. An investigation into the solid solution $xAg_2Nb_4O_{11}$–$(1-x)Na_2Nb_4O_{11}$ has shown that the progressive replacement of Ag^+ by Na^+ causes a reduction in T_C and that at a composition of $x=0.75$, there is a phase boundary between monoclinic and rhombohedral structures [6].

In the $xAg_2Nb_4O_{11}$–$(1-x)Na_2Nb_4O_{11}$ solid solution, there are therefore four known structural variants that exist as a function of temperature and composition, but their corresponding phase fields are unknown. In this work, the temperatures and compositions of the phase boundaries have been determined with the primary intention of producing a phase diagram for the solid solution to elucidate the sequences of phase transitions that can take place.

2. Materials and methods

Powders in the $xAg_2Nb_4O_{11}$–$(1-x)Na_2Nb_4O_{11}$ solid solution were made by a standard solid-state processing route. Ag_2O (99+%, Alfa Aesar), Nb_2O_5 (Puratronic, 99.9985%) and Na_2CO_3

* Corresponding author. Fax: +44 24 7615 0897.
E-mail address: d.i.woodward@warwick.ac.uk (D.I. Woodward).

0022-4596/$ - see front matter © 2012 Elsevier Inc. All rights reserved.
http://dx.doi.org/10.1016/j.jssc.2012.04.014

(BDH, 99%) were weighed out in stoichiometric amounts into batches of ~50 g. These were ball-milled for ~24 h in a high-density polythene pot with propan-2-ol and 10 mm diameter milling media. The slurry was dried at 70 °C and the resultant powder ground with a pestle and mortar and passed through a 250 μm mesh sieve. The mixed powders were reacted in a lidded Al_2O_3 crucible and heated at a ramp rate of 5 °C/min to 800 °C for 2 h, with the exception of compositions $x=0$ and 0.25 which were heated to 775 °C. After reacting, the crucible remained in the furnace which was left to cool with no power applied. Phase purity was assessed by powder X-ray diffraction (XRD). Only $Ag_2Nb_4O_{11}$ was found to be phase pure by XRD. All other compositions were found to contain weak peaks corresponding to the phase $Na_{13}Nb_{35}O_{94}$ [17].

XRD was performed using a Panalytical X'Pert Pro MPD with a curved Johansson monochromator producing Cu $K\alpha1$ radiation. An Anton Paar HTK1200N furnace was used to heat the samples above room temperature at a rate of 0.5 °C/min. Pawley refinements were performed on these data using Topas Academic 4.1 to produce lattice parameters [18]. Low-temperature XRD was performed on a Bruker D5005 diffractometer, equipped with an Oxford Cryosystems Phenix low-temperature stage which cooled the samples at a rate of 0.5 °C/min.

Differential scanning calorimetry (DSC) was performed using a Mettler Toledo DSC1 STARe system. Samples were weighed into Al pans, cooled to −150 °C, heated to 200 °C at a rate of 5 °C/min and cooled back down to −150 °C at the same rate.

Degradation of the natrotantite structure at elevated temperatures prevents the formation of dense ceramics, so where solid samples were required to be poled, powder of the relevant composition was mixed with an epoxy resin (M-Bond 610, Agar Scientific), centrifuged for 5 min at 40,000 RPM and cured for 4 h at 100 °C, using the technique reported by Carr [19]. One of the main benefits of using composites instead of porous ceramics is that the absence of air within the material means that high fields can be used without arcing. Silver paste (RS Components) was used to paint electrodes onto these composites, which were then poled for 10 min at room temperature at fields up to a maximum of 6 kV/mm. Values of d_{33}, the piezoelectric coefficient relating the charge generated on the faces normal to an applied force, were obtained using a YE2730A d_{33} meter (APC International, Ltd.). This method of mixing powder samples into a resin matrix creates a '0–3 composite', so-called because a representative cube of the composite comprises a dispersed piezoelectric phase with no connectivity in the three directions perpendicular to the cube faces, while the matrix phase has connectivity in all three directions [20].

Measurements of the low-temperature permittivity were performed on samples with compositions $x=0.25$ and $x=0.5$ in order to establish the temperatures of phase transitions taking place below room temperature. Test samples were made by pressing the reagents into pellets and reacting for 2 h at 825 °C. This resulted in a particularly porous ceramic but with sufficient structural integrity to be used in this test. The samples were fixed to a small stage using silver epoxy (RS Components) as both an adhesive and an electrode material and then a Physical Property Measurement System (Quantum Design) was used to cool the samples to −263 °C at 1 °C/min. The capacitance was measured *in-situ* with an Agilent 4294A Impedance Analyzer.

3. Results and discussion

3.1. Ferroelectric ↔ paraelectric transition

Table 1 shows the values of d_{33} recorded for composites in the series. These show that samples with compositions $x \geq 0.6$ are ferroelectric at room temperature, while those with compositions $x \leq 0.5$ are not. As samples $x \leq 0.7$ are monoclinic at room temperature, this shows that ferroelectricity persists into the monoclinic phase field. 0–3 composites containing 60 vol% $Pb(Zr_{1-x}Ti_x)O_3$ (PZT) have been found to have a d_{33} an order of magnitude lower than that of the corresponding ceramic [21]. The d_{33} of $Ag_2Nb_4O_{11}$ is therefore anticipated to be around 50 pC/N—similar to that of many perovskites.

Table 1
Piezoelectric coefficients for composites in the $xAg_2Nb_4O_{11}$–$(1-x)Na_2Nb_4O_{11}$ solid solution at room temperature. Where fields below 6 kV/mm are reported, the maximum applicable field was limited by sample conductance. The error in the reported d_{33} values is ±5%.

Composition, x	Maximum poling field (kV/mm)	d_{33} (pC/N)
0	6	0
0.25	6	0
0.5	6	0
0.6	4.3	0.8
0.65	6	0.4
0.7	3.9	1.0
0.75	2.3	2.5
1	6	3.4

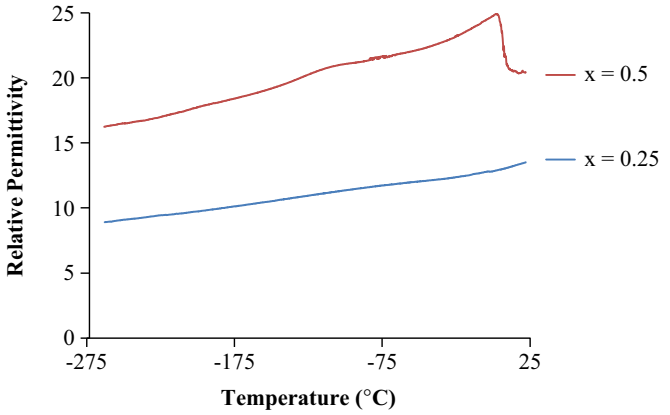

Fig. 1. Low-temperature permittivity obtained during cooling for ceramics with compositions $x=0.5$ and $x=0.25$. These data have not been corrected for porosity.

Low-temperature permittivity was used to locate the ferroelectric phase transition below room temperature (Fig. 1). The composition $x=0.5$ shows a peak in permittivity at ~2 °C, indicating the ferroelectric phase transition, while the composition $x=0.25$ shows no peak between room temperature and −263 °C, showing that the temperature of the ferroelectric phase boundary drops sharply for $x<0.5$. It was found that the temperature of the peak in the $x=0.5$ trace was repeatable to within ±15 °C.

3.2. Rhombohedral ↔ monoclinic transition

Powder XRD patterns of compositions across the series were used for Pawley refinements to obtain lattice parameters for each composition in the series. The volume per formula unit for each composition is plotted in Fig. 2. At $x=0.75$, where rhombohedral (R) and monoclinic (M) structures coexist, it is clear that the phase transition from R to M is accompanied by an increase in volume. It therefore follows that there should be an associated peak in DSC for R–M phase transitions. High-temperature XRD data of $Na_2Nb_4O_{11}$ ($x=0$) (Fig. 3) show peaks that split on transforming from R to M. These data show that the R–M phase transition is close to 80 °C for $Na_2Nb_4O_{11}$. DSC data for $x=0$ are shown in Fig. 4, where the only peak in this range has a mean

onset temperature of 80 (2) °C. It is concluded that this peak arises due to the R–M phase transition and its onset temperature can therefore be used to give a more precise measure of the phase transition temperature than XRD. The physical origin of the peak at ~70 °C in the heating curve is unknown.

Fig. 5 shows that this peak moves to lower temperatures as x increases. The mean onset values derived from these peaks for the corresponding R–M transition are given in Table 2. No relevant peak was observed in DSC for $x=0.75$, but at room temperature, XRD shows the presence of both R and M phases. Low-temperature XRD of $x=0.75$ shows that both sets of peaks persist to −253 °C (Fig. 6), indicating that the R–M phase boundary at $x=0.75$ is virtually temperature-independent. Perhaps the best-known example of a temperature-independent phase boundary is in PZT, at which piezoelectric properties are found to be maximised [22,23]. It is yet to be shown whether piezoelectric properties are maximised at this, a phase boundary in a different structural system.

3.3. *R3c↔R3 transition*

DSC shows strong peaks in the heating and cooling sections for $Ag_2Nb_4O_{11}$ with a mean onset temperature of −62 (1) °C (Fig. 7) and it is assumed that these peaks are associated with the volume change of the *R3c*–*R3* phase transition. This transition was found to be present in all samples with compositions $x \geq 0.75$, i.e. those with rhombohedral symmetry at room temperature (Fig. 8). The temperature of this phase transition is almost independent of composition, varying by only 2 °C across the four samples (Table 3). Samples with compositions $x \leq 0.7$ have no peaks that could correspond to this transition and so it must be concluded that the phase transition mechanism does not take place in the

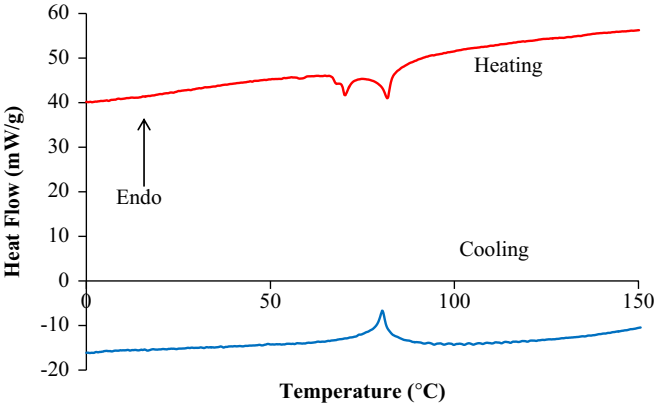

Fig. 4. DSC heating and cooling data for $Na_2Nb_4O_{11}$ ($x=0$) showing peak due to R–M transition.

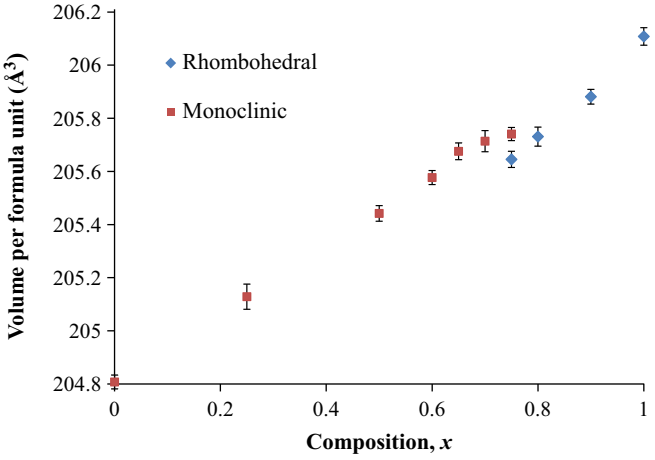

Fig. 2. Volume per formula unit of compositions in the $xAg_2Nb_4O_{11}$–$(1-x)Na_2Nb_4O_{11}$ series derived from Pawley refinements.

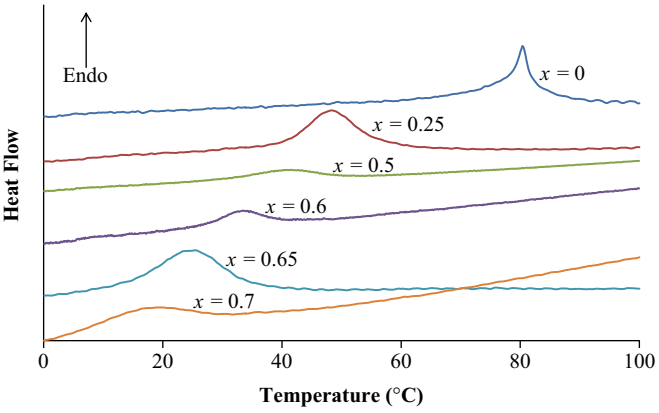

Fig. 5. DSC cooling data for compositions in the $xAg_2Nb_4O_{11}$–$(1-x)Na_2Nb_4O_{11}$ series.

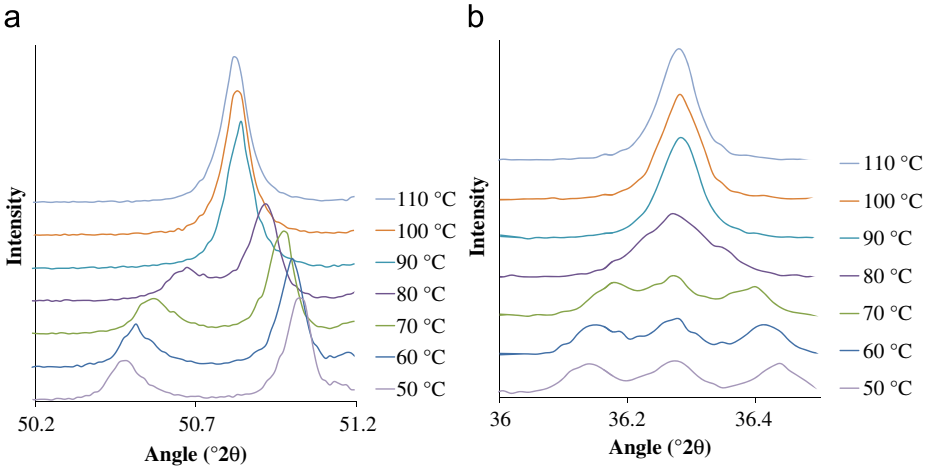

Fig. 3. High-temperature XRD data from $x=0$ ($Na_2Nb_4O_{11}$) showing the evolution of two key peaks with temperature: (a) $\{3\,0\,0\}_R$ splits into $\{60\bar{2}\}_M$ and $\{\bar{3}31\}_M$ peaks (b) $\{\bar{1}26\}_R$ splits into $\{3\,1\,1\}_M$, $\{3\bar{1}3\}_M$ and $\{0\,2\,2\}_M$ peaks on cooling through the R–M phase transition.

Table 2
Mean onset temperatures for R–M phase transition from DSC data.

Composition, x	Mean onset temperature (°C)
0.7	30 (5)
0.65	34 (5)
0.6	39 (5)
0.5	47 (5)
0.25	55 (5)
0	80 (2)

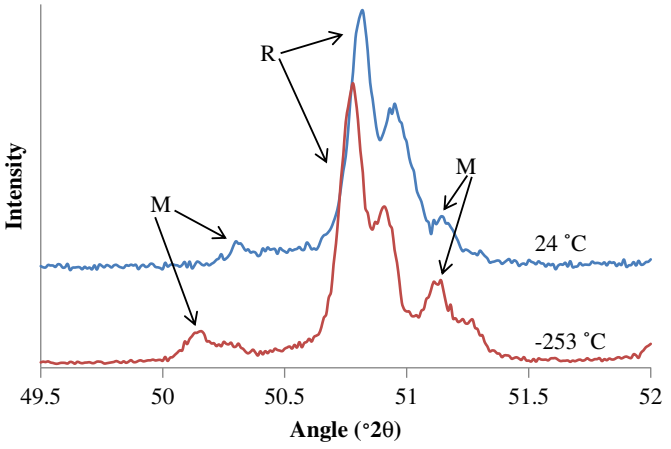

Fig. 6. XRD of $x=0.75$ sample showing the presence of $\{3\,0\,0\}_R$, $\{60\bar{2}\}_M$ and $\{\bar{3}31\}_M$ peaks corresponding to both R and M phases at 24 and −253 °C.

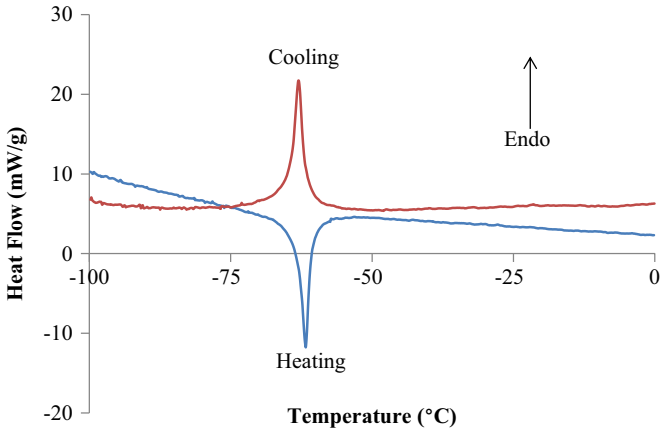

Fig. 7. DSC heating and cooling curves for $Ag_2Nb_4O_{11}$ ($x=1$) with peak due to $R3c$–$R3$ phase transition.

monoclinic variant. Where the $R3c$–$R3$ phase boundary meets the R–M phase boundary, there is therefore a triple point.

4. Conclusions

High- and low-temperature X-ray diffraction, differential scanning calorimetry, low-temperature permittivity and room-temperature piezoelectric techniques have been used to plot a phase diagram as a function of temperature for compositions in the natrotantite-structured system $xAg_2Nb_4O_{11}$–$(1-x)Na_2Nb_4O_{11}$ (Fig. 9). There are three separate phase transition types: (1) paraelectric–ferroelectric, (2) rhombohedral–monoclinic and (3) a phase transition within the ferroelectric rhombohedral zone between the space groups $R3c$ and $R3$.

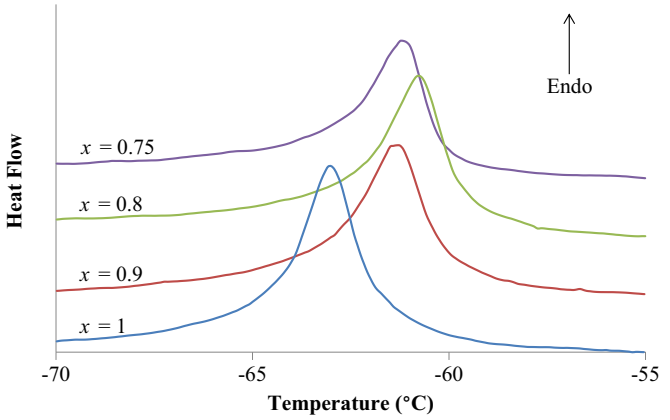

Fig. 8. DSC cooling curves for compositions with $x \geq 0.75$ showing peaks due to $R3c$–$R3$ phase transition.

Table 3
Mean onset temperatures for $R3c$ – $R3$ phase transition from heating and cooling DSC data.

Composition, x	Mean onset temperature (°C)
1	−62(1)
0.9	−61(1)
0.8	−61(1)
0.75	−61(1)

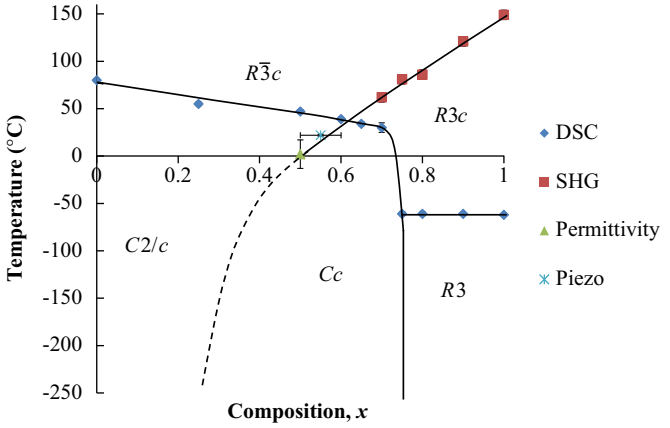

Fig. 9. Phase diagram of the $xAg_2Nb_4O_{11}$–$(1-x)Na_2Nb_4O_{11}$ solid solution. SHG data taken from [6].

The parent phase for all structures in this solid solution, and by extension, all natrotantite-structured materials, has space group $R\bar{3}c$, analogous to the cubic parent structure of perovskites with space group $Pm\bar{3}m$. Ferroelectricity is present in both rhombohedral and monoclinic variants but no evidence of ferroelectricity is found for compositions $x \leq 0.25$. The rhombohedral–monoclinic phase boundary appears temperature-independent for composition $x=0.75$ below room temperature. The $R3$–$R3c$ phase boundary appears to be independent of composition but does not extend into the monoclinic phase field and it is concluded that a triple point is formed where it meets the rhombohedral–monoclinic phase boundary.

Acknowledgments

The PANalytical MPD diffractometer used in this research was obtained though the Science City Energy Futures Project: Hydrogen Energy, with support from Advantage West Midlands (AWM).

The DSC, PPMS and Impedance Analyzer used in this research were obtained though the Science City Advanced Materials project: "Creating and Characterizing Next Generation Advanced Materials" project, with support from Advantage West Midlands (AWM) and partly funded by the European Regional Development Fund (ERDF).

References

[1] M.C. Stennett, I.M. Reaney, G.C. Miles, D.I. Woodward, A.R. West, C.A. Kirk, I. Levin, J. Appl. Phys. 101 (2007) 104114.
[2] V.A. Isupov, Tech. Phys. 42 (1997) 1155–1157.
[3] M.T. Weller, R.W. Hughes, J. Rooker, C.S. Knee, J. Reading, Dalton Trans. 19 (2004) 3032–3041.
[4] R.E. Newnham, R.W. Wolfe, J.F. Dorrian, Mater. Res. Bull. 6 (1971) 1029–1040.
[5] N. Masó, D.I. Woodward, P.A. Thomas, A. Várez, A.R. West, J. Mater. Chem. 21 (2011) 2715–2722.
[6] D.I. Woodward, P.A. Thomas, Appl. Phys. Lett. 98 (2011) 132904.
[7] T.S. Ercit, F.C. Hawthorne, P. Černý, Bull. Mineral. 108 (1985) 541–549.
[8] R. Mattes, J. Schaper, Rev. Chim. Miner. 22 (1985) 817–820.
[9] L. Jahnberg, J. Solid State Chem. 1 (1970) 454–462.
[10] L. Jahnberg, M. Sundberg, J. Solid State Chem. 100 (1992) 212–219.
[11] O. Palasyuk, A. Palasyuk, P.A. Maggard, Inorg. Chem. 49 (2010) 10571–10578.
[12] VonE. Bayer, R. Gruehn, Z. Anorg. Allg. Chem. 507 (1983) 149–154.
[13] C. Zheng, A.R. West, J. Mater. Chem. 1 (1991) 163–167.
[14] N. Masó, A.R. West, J. Mater. Chem. 20 (2010) 2082–2084.
[15] E. Irle, R. Blachnik, B. Gather, Thermochim. Acta 179 (1991) 157–169.
[16] N. Masó, D.I. Woodward, A. Várez, A.R. West, J. Mater. Chem. 21 (2011) 12096–12102.
[17] D.C. Craig, N.C. Stephenson, J. Solid State Chem. 3 (1971) 89–100.
[18] A. A. Coelho, TOPAS-Academic v4.1, 〈http://www.topas-academic.net〉 (2007). Last accessed 09.02.12.
[19] M.J. Carr, J. Electron Micr.. Microsc. Tech. 2 (1985) 439–443.
[20] R.E. Newnham, D.P. Skinner, L.E. Cross, Mater. Res. Bull. 13 (1978) 525–536.
[21] I. Babu, D.A. Van den Ende, G. De With, J. Phys. D: Appl. Phys. 43 (2010) 425402.
[22] B. Jaffe, W.R. Cook, H. Jaffe, Piezoelectric ceramics, Academic Press Inc., London, 1971.
[23] D.A. Berlincourt, C. Cmolik, H. Jaffe, Proc. I. R. E. 48 (1960) 220–229.